$$= A\int_0^\infty K(|z-L-y|)e_0(L+y)\,dy + \int_0^\infty K(|z-L-y|)\,dy\int_0^L G(L+y,z'')J(z'')\,dz''. \tag{A4}$$

In the integral on the left-hand side of (A4), let $L-z'=y$ be the integration variable. That integral becomes

$$\int_0^L K(|z-L+y|)h(y)\,dy\ ,$$

and now replacing $L-z$ by z everywhere in (A4) gives

$$\left(\frac{d^2}{dz^2}+k_0^2\right)h(z)+\int_0^L K(|z-y|)h(y)\,dy = A\int_0^\infty K(|z+y|)e_0(L+y)\,dy + \int_0^\infty K(|z+y|)\,dy\int_0^L G(L+y,z')J(z')\,dz' \equiv Aj_1(z)+\int_0^L \mathcal{G}(z,z')J(z')\,dz'\ , \tag{A5}$$

where $j_1(z)$ and $\mathcal{G}(z,z')$ are defined as (3.10).

[1]For an early review see E. A. Kaner and V. F. Gantmakher, Usp. Fiz. Nauk **94,** 193 (1968) [Sov. Phys. Usp. **11,** 81 (1968)].

[2]D. S. Falk, B. Gerson, and J. F. Carolan, Phys. Rev. B **1,** 406 (1970).

[3]B. Perrin, G. Weisbuch, and A. Libchaber, Phys. Rev. B **1,** 1501 (1970).

[4]G. A. Baraff and T. G. Phillips, Phys. Rev. Lett. **24,** 1428 (1970).

[5]L. T. Wood and J. D. Gavenda, Phys. Rev. B **2,** 1492 (1970).

[6]T. G. Phillips, G. A. Baraff, and P. H. Schmidt, Phys. Rev. Lett. **25,** 930 (1970).

[7]J. F. Cochran, Can. J. Phys. **48,** 370 (1970).

[8]J. O. Henningsen and D. S. Falk, Phys. Rev. Lett. **26,** 1174 (1971).

[9]R. F. Milligan and T. G. Castner, Jr., Phys. Rev. Lett. **26,** 1560 (1971).

[10]T. G. Phillips, G. A. Baraff, and P. H. Schmidt, Phys. Rev. B **5,** 1283 (1972).

[11]P. M. Platzman and S. J. Buchsbaum, Phys. Rev. **132,** 2 (1963).

[12]G. A. Baraff, Phys. Rev. **178,** 1155 (1969). See Appendix.

[13]P. R. Antoniewicz, Phys. Rev. **185,** 863 (1969).

[14]G. A. Baraff, J. Math. Phys. **9,** 372 (1968).

[15]G. A. Baraff, Phys. Rev. **167,** 625 (1968).

[16]V. F. Gantmakher and E. A. Kaner, Zh. Eksp. Teor. Fiz. **48,** 1572 (1965) [Sov. Phys. JETP **21,** 1053 (1965)].

[17]G. E. H. Reuter and E. H. Sondheimer, Proc. R. Soc. A **195,** 336 (1948).

[18]R. B. Dingle, Physica (Utr.) **19,** 311 (1953).

[19]The question of whether election trajectories double back on themselves involves both the details of Fermi-surface shape and the direction of the steady magnetic field, both being quantities which govern the conductivity.

[20]G. A. Baraff, J. Math. Phys. **11,** 1938 (1970); J. Math. Phys. **13,** 927E (1972).

[21]R. Kalaba, J. Math. Phys. **11,** 1999 (1970).

[22]Ralph M. Wilcox, J. Math. Phys. **12,** 1195 (1971).

[23]S. W. Lee (unpublished) has devised a more conventional Wiener–Hopf technique than that used in Refs. 14 and 15.

PHYSICAL REVIEW B VOLUME 7, NUMBER 2 15 JANUARY 1973

Self-Diffusion along Dislocations in Single-Crystal Au Films

D. Gupta

IBM Thomas J. Watson Research Center, Yorktown Heights, New York 10598

(Received 21 June 1972)

Self-diffusion measurements over the temperature range 247–352 °C have been made on single-crystal Au films of 2-μ thickness grown epitaxially onto (001) MgO substrates, using Au^{195} radioactive tracer and rf sputter-etching techniques for serial sectioning. The penetration profiles revealed shallow lattice diffusion and a much deeper tracer penetration down dislocations; the former is significantly enhanced by diffusion in dislocations. The activation energy Q_d and the combined preexponential factor $A_dD_d^0$ for self-diffusion along dislocations are found to be 1.16 ± 0.02 eV and 5×10^{-16} cm^4/sec, respectively. From the enhanced lattice diffusion observed in the first stage of the penetration profiles, a dislocation density of $\sim10^{11}$ lines/cm^2 could also be evaluated for the single-crystal films. The data compare well with other fcc metals and appear to favor a vacancy diffusion mechanism.

I. INTRODUCTION

It is now well established that self-diffusion in the regions of dislocations or grain boundaries in fcc metals is orders of magnitude faster than in the lattice.[1] Self-diffusion measurements, commonly involving the transport of tracer atoms, have been successfully employed to measure these contributions. For isolated dislocations, diffusion is measured in the form of a combined parameter P_d (cm^4/sec) defined as

$$P_d = D_d A_d\ , \tag{1}$$

where D_d is the self-diffusivity along dislocations and A_d (cm^2) is the effective cross-sectional area of the dislocation core. Diffusion along closely spaced arrays of parallel dislocations constituting low-angle boundaries has also been measured by treating these planar arrays as a homogeneous grain-boundary slab. The model leads to another combined parameter P_b (cm^3/sec) for boundary diffusion given by

$$P_b = \delta D_b, \tag{2}$$

where the subscripts now refer to the boundary diffusion and δ (cm) is the half-width of the slab. Equations (1) and (2) ordinarily lead to $D_d = D_b$ (cm^2/sec) since P_b and P_d are related only by the dislocation spacing l_d (cm) as

$$P_b l_d = P_d. \tag{3}$$

The temperature dependence of the combined parameters P_d and P_b is due entirely to the temperature dependence of the diffusivities D_d and D_b expressed by the Arrhenius parameters, the preexponential factor $D_d^0 = D_b^0$, and the activation energies Q_b and Q_d, which should be equal if Eq. (3) is to be valid. Thus designating $P_d^0 = A_d D_d^0$ and $P_b^0 = l_d \delta D_b^0$, Eqs. (1) and (2) may be rewritten as

$$P_d = P_d^0 e^{-Q_d/RT}, \tag{4}$$

$$P_b = P_b^0 e^{-Q_b/RT}. \tag{5}$$

In a recent survey of self-diffusion measurements along dislocations in fcc metals, Balluffi has found the data to be relatively sparse and often imprecise.[2] Based on rather selective data, his general conclusions are that fast diffusion occurs along dislocations in a narrow region near the core. Also, the observed activation energies are characteristically smaller in comparison to the lattice self-diffusion, being ~ 40% for single nondissociated dislocations and 60–80% for dissociated ones. The difference is attributable to a larger core distortion in the former case. In general, a vacancy mechanism has been favored for diffusion along isolated dislocations and dislocation arrays. The notable exclusions of the data from those considered in arriving at the above conclusions were the *direct* measurements of self-diffusion along edge dislocations in Ni and Ni-Co alloy of Birnbaum and co-workers.[3,4] Both yield values of P_d^0 several orders of magnitude larger than obtained elsewhere.[5–10] The scatter in the parameter P_d^0 even among the latter group of investigations[5–9] is some 4 orders of magnitude.

It is therefore obvious that the problem of dislocation pipe diffusion in fcc metals is far from settled and precise new measurements are desirable. Gold in particular is an attractive candidate because of the valuable information already available on self-diffusion parameters in the lattice and on the behavior of quenched-in defects.[11–13]

Attempts have recently been made[14,15] to measure self-diffusion in Au single crystals at low temperatures using anodic oxidation-stripping and electrolytic techniques for serial sectioning. An activation energy for self-diffusion along dislocations equal to 1.2 eV was reported[15] by observing enhanced lattice diffusion and attributing the difference to diffusion in dislocations; however, the preexponential factor P_d^0 was not determined.

This investigation was aimed at measuring self-diffusion along dislocations in Au unambiguously at temperatures substantially below $0.5T_m$ (half the absolute melting temperature) where a dislocation mode of diffusion may be expected to be dominant. It was also desirable to maintain a high dislocation density in the specimens with well-defined stable geometry so that high radio counting rates may be maintained even at large tracer-penepenetration depths. Since epitaxial films are known to have a rather high dislocation and stacking fault density[16,17] in the range 10^{10}–10^{11} cm^{-2}, single-crystal Au film specimens grown epitaxially onto MgO substrates of ⟨001⟩ orientation were used. The dissociated dislocations in the (001) films lie in {111} planes with their lines along a ⟨211⟩ direction such that they thread the film thickness. Any meaningful radioactive tracer diffusion in thin films necessarily involves submicron sectioning since films themselves are typically only microns thick and diffusion depths have to be maintained shallower at the temperatures of interest to preserve the semi-infinite boundary conditions for the specimens. Obviously, mechanical methods of material removal could hardly be considered. The electrochemical techniques used earlier[13–15] were found to be inadequate since dislocation pipes were preferentially attacked and, owing to the high dislocation density present in the films, large holes developed in the film with accompanying loss of adhesion to the substrate. These difficulties have been surmounted by the development of a novel technique for serial sectioning at submicron level using an rf sputter-etching procedure in an argon glow discharge which is quick and reproducible. A brief description of this rapid and reproducible technique has been given elsewhere[18] and a complete account is expected to be available in the near future.[19] By employing this technique for material removal and collection, it was possible to take sections of 30-Å thickness with ease.

II. EXPERIMENTAL PROCEDURES

A. Specimens and Diffusion of Tracers

Single-crystal thin-film Au specimens ($\frac{3}{4}$-in. diameter and 2 μ thick) grown epitaxially onto (001)

MgO substrates were used for the diffusion measurements. Gold deposition was carried out by rf sputtering with a peak-to-peak voltage of 2400 V at 13.56 MHz. The as-received substrates, with a 1-μin. surface finish, were lightly etched in concentrated phosphoric acid preheated to 175 °C to eliminate cold work. The substrates were Ga-backed and mounted on a gold-plated molybdenum substrate holder. The Au cathode source for the film deposits was of 99.999+% purity.[20] The chamber was prepumped to 5×10^{-8} Torr, and the substrates brought to 450 °C and charged with 2.5×10^{-3}-Torr gas pressure of Ar of 99.999+% purity. The Au cathode and the substrates were sputter-cleaned *in situ* for 15 min by reversing the potential between the two electrodes alternately and collecting the sputtered-off material onto a grounded intervening shutter which also served as a collector for contaminants. The Au film deposition to 2-μ thickness was carried out onto the substrates with a bias of − 50 V. The accumulation rate was typically 17.4 Å/sec at a power density of 2.5 W/cm^2. The films, thus deposited, were firmly bonded to the MgO substrates with a mirrorlike specular surface reflection.

The Au films were examined for their epitaxial character by matching back-reflection x-ray Laue spots in the Au deposit with those in the MgO substrates. Electron micrographs of the replicas of the film surfaces showed only the presence of twin and traces of (111) twin plane with the film surface. All the films had (001) plane parallel to their surfaces.[21]

Since the surfaces of the films were excellent and the subsequent diffusion temperatures were lower than the film-deposition temperature, no prior preparation of the specimens, such as polishing or stress relieving, was considered necessary. An activity corresponding to 2 μC of carrier-free Au^{195} (180-day, 0.067-MeV γ) radioactive isotope[22] was electroplated, which constituted less than a monoatomic layer of the tracer on the film surface. Consequently the planar thin-layer boundary condition for geometry was fulfilled for the tracer deposit. The specimens were encapsulated in quartz and annealed in a furnace controlled to ±0.1 °C. Warm-up time corrections were made for short-diffusion anneals, and at the termination of an anneal a sharp cutoff was obtained by quenching the capsules in cold water.

B. Sectioning and Counting

Submicron sectioning of the diffused specimens was achieved by rf reverse sputtering.[18,19] An Ar gas glow discharge with a peak-to-peak voltage value of 1000 V at 13.56 MHz was used to remove thin layers of material from the films; the sputtered-off material was collected onto aluminum disk planchets attached to the anode. To speed up the sectioning operation by reducing the number of pumpdown cycles, a multianode apparatus was employed, containing six planchets on a rotating head. Hence, six consecutive sections could be obtained in a single pumpdown. The rf power supply was stabilized to within ±1% of voltage. During sectioning, a precise control on the geometry of the specimen in relation to the electrodes was maintained to ensure that a constant fraction (~30%) of sputtered material was collected in successive sections. The duration of etching varied from 15 seconds to several minutes. The surface temperature of the specimen being sputtered was measured earlier[23] and was found to level off to about 120 °C within a few minutes, which is at least 100 °C below the lowest of the diffusion temperatures of this investigation. Consequently, no significant perturbation of the tracer profile caused by heating up of the specimens during sputtering is expected.

For the thickness determination of the material removed, the Au thin-film samples, along with the substrate, were weighed in a Sartorius microbalance. By virtue of the high density of Au, the thickness measurement of sections from successive weight determinations posed no problem. The penetration distance, therefore, could be computed from the cumulative weight loss of the specimen between successive sputtering cycles, the diameter of the film, and the density of Au metal. Since the Au film did not cover the MgO substrate completely, some sputtering of the substrate also took place. However, a correction for this account was found to be insignificant owing to the low density of MgO and its low sputtering rate, which was typically < 0.1 Å/sec, in comparison to 2 Å/sec for Au.

A major concern in sectioning the film specimens was the possibility of violating the semi-infinite boundary condition for the thickness of the specimen in comparison to the absolute depth of the tracer penetration. The time and temperature for the diffusion anneals, therefore, had to be so selected that the tracer-penetration depth was no more than ~30% of the total film thickness. The residual activity in the specimens was monitored continually during the sectioning operation and when it dropped to less than 1% of the plated activity within the first 30% of the film thickness, the above condition was considered to have been fulfilled. The narrow range of the temperature of the diffusion measurements in this investigation reflects the limitations imposed by the semi-infinite boundary condition of the specimen in relation to tracer penetration at the high temperatures and the avoidance of appreciable heating of the sample during sputtering at the low temperatures.

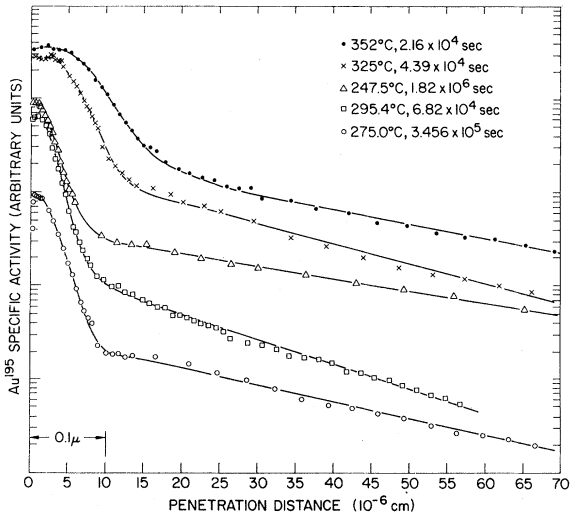

FIG. 1. Au^{195} tracer-penetration profiles in (001) single-crystal Au films on MgO substrates. The log specific activities are plotted against the *penetration distance*.

Counting of Au^{195} (0.067 MeV γ) was carried out using a single-channel scintillation spectrometer with a pulse-height analyzer and a 2-in.-diam, $1\frac{1}{2}$-in.-deep NaI(Tl) crystal detector. A window was set on the 0.067-MeV γ peak and the statistical errors in counting were kept below 1%. The diffused sections in the form of collected material onto the aluminum planchets could be directly counted without any further processing. The deposit had well-defined reproducible geometry and the nuclear absorption was almost totally absent since the deposit thickness was hardly a monoatomic layer

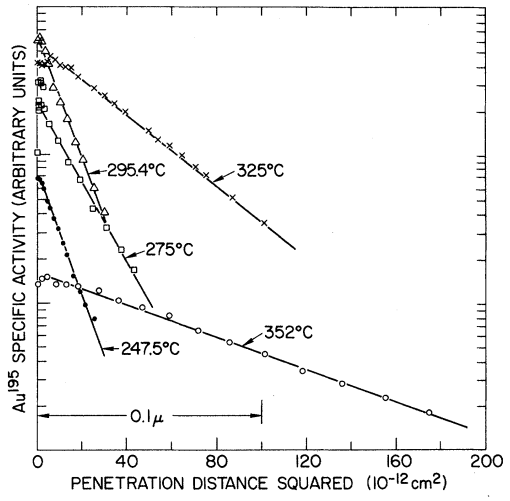

FIG. 2. Curved segments of the Au^{195} tracer profiles in Fig. 1 replotted in *penetration distance squared* to reveal their Gaussian nature.

III. RESULTS

Au^{195} tracer-penetration profiles, plots of the log of the specific activity versus the penetration distance, at five temperatures in the range of (247.5–352) °C are shown in Fig. 1. All these measurements were made below $0.5T_m$, where contributions from both the lattice and dislocations may be expected. It is seen in Fig. 1 that the profiles have initial curved segments which are followed by clearly linear tails extending to large depths in the films; the former appear to be semi-parabolic in shape.

To check the precise nature of the curved segments of the profiles at the shallow ends, the data are plotted in the penetration distance squared in Fig. 2. It is seen that the curved portions of the profiles in Fig. 1 have reduced to excellent straight lines up to the points of inflections, indicating early lattice-type diffusion in these single-crystal films, Consequently, extraction of the apparent lattice diffusivity D_{app} was performed according to the instantaneous thin-planar-source solution

$$C_l = [C_l^0/(\pi D_{app}\, t)^{1/2}]e^{-x^2/4D_{app}\, t}, \qquad (6)$$

where C_l is the concentration of the tracer at penetration distances x and time t, and C_l^0 at $x=0$ and $t=0$. The least-squares values of the apparent lattice diffusivities obtained from the straight lines

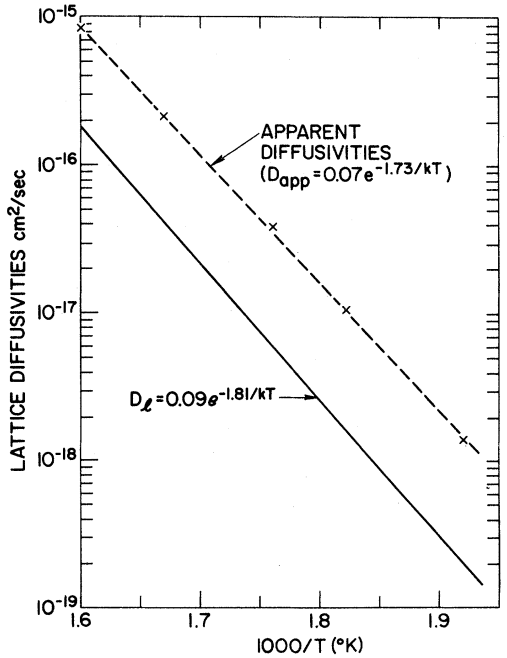

FIG. 3. Comparison of the apparent lattice diffusivities extracted from the tracer profiles in Fig. 2 (dashed line) with the actual lattice self-diffusion data of Makin *et al.* (Ref. 24).

TABLE I. Apparent self-diffusion coefficients and the calculated dislocation densities.

Temp. (°C)	D_l(cm^2/sec)[a]	D_{app}(cm^2/sec)[b]	$(D_l t)^{1/2}$(Å)	$f=(D_{app}-D_l)/D_d$[c]	$\sim \rho_d$(cm^{-2})
352.0	1.88×10^{-16}	8.30×10^{-16}	202	1.05×10^{-4}	1.2×10^{11}
325.1	4.10×10^{-17}	2.16×10^{-16}	134	7.1×10^{-5}	8.6×10^{10}
295.4	6.35×10^{-18}	3.80×10^{-17}	66	5.7×10^{-5}	6.8×10^{10}
275.0	1.63×10^{-18}	1.05×10^{-17}	75	3.7×10^{-5}	4.5×10^{10}
247.5	2.13×10^{-19}	1.36×10^{-18}	62	1.2×10^{-5}	1.5×10^{10}

[a]Calculated from $D_l = 0.091\ e^{-1.81/kT}$ (Ref. 24).
[b]Temperature dependence expressed by $0.07(\pm0.01)e^{-1.73(\pm02/kT)}$.
[c]$D_d = D_b$ in Table II assuming $\delta = 1.5\times10^{-8}$ Å.

in Fig. 2 are listed in Table I and displayed in Fig. 3; their temperature dependence is expressed by $D_{app} = 0.07\ e^{-1.73/kT}$. The lattice-diffusion coefficients D_l computed from the known activation energy $Q_l = 1.81$ eV and the preexponential factor $D_l^0 = 0.091$ cm^2/sec for self-diffusion in Au[24] are also shown. This extrapolation is quite accurate since the subsequent self-diffusion measurements[11–13] also have the same Arrhenius dependence.

Extraction of diffusivities from the linear tails in Fig. 1 requires some assumptions to be made on the geometrical arrangement of the dislocations. If the dislocations are considered as planar parallel arrays, the homogeneous grain-boundary slab analogy is applicable and then the combined parameter P_b (cm^3/sec) is the measured quantity. The data may be accordingly processed using either Fisher's[25] or Whipple's[26] analyses. Alternatively, for diffusion in isolated dislocations Smoluchowski's[27] model should be used, and in that event P_d (cm^4/sec) is the evaluated parameter according to Eq. (1). Because of the possibility of the results being influenced by the underlying assumptions in the two analyses, which will be discussed later, it was considered appropriate to use both analyses.

The parameters $\beta = \delta D_b / 2D_l(D_l t)^{1/2}$ and P_b were computed from the linear portions of the penetration profiles in Fig. 1 using Whipple's exact solution and the graphical procedure of Canon and Stark.[6] Values of $P_b = \delta D_b$ and β are listed in Table II. It may be noted that while Whipple's exact analysis is used here in totality, Fisher's analysis is equally precise in most cases in view of the large values of β ($\gg 100$) used in this investigation. However, some discrepancy was observed in the 352 °C anneal for which β turned out to be only 120 and consequently Fisher's analysis was inaccurate.

For the isolated-dislocation-pipe-diffusion model, Pavlov[28] and Brebec[29] have developed the expression

$$\frac{\partial \ln(C_d/C_d^0)}{\partial x} = -\left(\frac{8\ D_l\ \phi(t)}{\pi^2\ A_d\ D_d}\right)^{1/2}, \tag{7}$$

where C_d is the tracer concentration in and around dislocations at penetration distance x and time t and C_d^0 is the concentration for $x=0$ and $t=0$. The quantity ϕ is a function of $D_l\ t/r_0^2$, r_0 being an assumed radius of the pipe; values of ϕ are available in tabular form.[28] The combined parameter $P_d = A_d D_d$ obtained from the least-squares slopes of the linear portions of the profiles in Fig. 1 is also given in Table II. The parameters for dislocation-pipe diffusion are $\delta D_b^0 = 1.9\times10^{-10}$ cm^3/sec and $Q_b = 1.16\pm0.02$ eV for Whipple's exact solution, assuming the homogeneous boundary-slab model, and $A_d D_d^0 = 10^{-17}$ cm^4/sec and $Q_d = 1.2\pm0.1$ eV for isolated dislocations geometry. It is seen that the deviation from an Arrhenius dependence in the latter case is relatively large.

TABLE II. Combined self-diffusion coefficients along dislocations.

	Homogeneous slab geometry		Isolated dislocation geometry		
Temp. (°C)	$\beta = P_b/2D_l(D_l t)^{1/2}$	P_b (cm^3/sec) ±10%	$D_l t/r_0^2$	ϕ	P_d (cm^4/sec) ±10%
352.0	120	9.15×10^{-20}	1.96×10^4	0.46	6.90×10^{-26}[a]
325.0	335	3.68×10^{-20}	8.68×10^3	0.49	6.21×10^{-27}[a]
295.4	1150	9.61×10^{-21}	2.09×10^3	0.58	9.41×10^{-28}
275.0	1470	3.60×10^{-21}	2.72×10^3	0.55	3.81×10^{-28}
247.5	5230	1.39×10^{-21}	1.87×10^3	0.58	1.29×10^{-28}
	$Q_b = 1.16\pm0.02$ eV			$Q_d = 1.2\pm0.1$ eV	
	$P_b^0 = 1.9\times10^{-10}$ cm^3/sec (±50%)			$P_d^0 = 1.0\times10^{-17}$ cm^4/sec (±50%)	

[a]Excluded from activation-energy calculation as they were substantially off.

IV. DISCUSSION

A. Resolution of Various Modes of Diffusion

The critical factors in this investigation have been the excellent resolution of the microsectioning technique and use of thin Au films. Since a section depth of less than 30 Å was possible, the diffusion distance, as indicated by $(D_l t)^{1/2}$, could be kept at ~100 Å. Consequently, a high resolution between the lattice and dislocation modes of diffusion could be achieved. The resolution obtained in microsectioning also made self-diffusion measurements possible at temperatures less than $0.4T_m$. The use of epitaxially grown Au films containing high dislocation densities, on the other hand, resulted in a high enough tracer activity for the accurate determination of diffusion tails. It is of interest to examine the experimental conditions which lead to the resolution seen in Fig. 1.

The entire temperature range of the present Au self-diffusion measurements falls in the mixed or type-B diffusion category of the general scheme of diffusion kinetics proposed by Harrison.[30] The type-B diffusion is non-Fickian in character and the plots of log (tracer activity) versus penetration distance are typically linear rather than parabolic in nature. It consists of restricted lattice diffusion and marked tracer penetration along dislocations and is characterized by the inequality

$$\delta < (D_l t)^{1/2} \ll l_d. \tag{8}$$

The physical meaning of the above inequality is that the tracer atoms in one dislocation pipe cannot travel to the other neighboring pipes. In view of $l_d \sim 500$ Å corresponding to a dislocation density of 10^{10}-10^{11} cm^{-2} and $(D_l t)^{1/2} \sim 100$ Å (Table I), the above inequality is satisfied in the present experiments. The observation of diffusion tails which are linear in the penetration distance is, in view of Harrison's criterion, reasonable.

As seen in Fig. 3, the diffusivities extracted from the curved sections of the penetration profiles *do not* match the known temperature dependence of the lattice diffusion in Au. Owing to the presence of dislocations on the films, the lattice diffusion, in general, is expected to be enhanced by Hart's short-circuiting process[31] according to

$$D_{\text{app}} = D_l + fD_d, \tag{9}$$

where D_{app} is the enhanced lattice diffusivity, f the fraction of atoms in dislocation pipes, and D_d the dislocation-pipe diffusivity. A necessary condition for the observation of Hart's short circuiting given by Ruoff and Balluffi[32] is

$$2(D_l t)^{1/2} > l_d. \tag{10}$$

Although the above inequality is not satisfied in the present case, enhanced lattice diffusion is nevertheless indicated in Fig. 3. While examining the inequality (10), Ruoff and Balluffi and also Harrison[30] suggested that a short-circuiting behavior may be possible in the presence of moving dislocations having appreciable thermal vibrational motion. The randomization of short circuiting is thus carried out by the visitations of the tracer atoms by the moving dislocations, rather than the other way around, regardless of the above inequality. Pashley has observed dislocation motion in thin single-crystal films of Au using transmission electron microscopy.[17] Two additional factors in this regard may also be mentioned: (a) the possibility of a nonuniform surface distribution of the radioactive tracer, particularly in the vicinity of the dislocation pipes, and (b) the averaging of all the tracer atoms in the sectioning operation, as they may not all meet the short-circuiting paths equally. Since on the average only ~10^{-2} atomic layers of carrier-free Au^{195} radiotracer atoms were deposited onto the film surface, in all probability the surface distribution was nonuniform and sizable tracer accumulations occurred in the high-energy regions of the dislocation pipes. Following diffusion, the situation could have manifested itself in a smaller effective l_d for the purpose of lattice-diffusion enhancement and possibly validating the inequality (10). Morrison and co-workers[33,34] have also observed enhanced lattice diffusion in Ag and Au despite a noncompliance of the necessary condition. They concluded that the inequality (10) is indeed too stringent and Hart's short circuiting according to Eq. (9) will be valid as long as the time spent by tracer atoms in dislocations is ft when averaged over all tracer atoms in any section at depth x. It may be noted that the over-all conditions are very favorable in thin films for lattice-diffusion enhancement in view of a large $f \sim 10^{-5}$ by virtue of a high density of dislocations, and the diffusion data in this investigation seem to corroborate the view that factors other than the inequality (10) may be equally important. Indeed, had inequality (10) been satisfied in the present case, no resolution between the two segments of profiles shown in Fig. 1 would have been possible.

B. Parameters for Dislocation-Pipe Diffusion: Q_d, P_d^0, P_b^0, and A_d

As mentioned earlier in Sec. III, the interpretation of the diffusion data is influenced by the underlying assumptions made concerning the geometrical arrangement of dislocations. To obtain a better quantitative insight, both the homogeneous slab geometry and Smoluchowski's isolated dislocation model have been used for data analysis. The question of the applicability of these models along with their respective solutions—Fisher[26] or Whipple[27] in the former case, and Pavlov[28] in the lat-

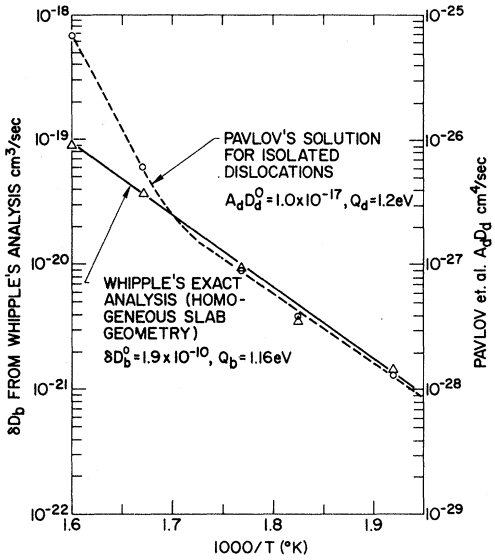

FIG. 4. Arrhenius nature of the combined self-diffusion coefficients along dislocations in (001) Au films. The data are obtained from the linear portions of tracer profiles in Fig. 1 and examined for alternative geometry of dislocations.

ter—now requires attention. In the first place, there has been some question as to whether the homogeneous slab geometry is applicable for a boundary containing widely spaced dislocation cores.[27] This assumption has been used earlier by Ghostagore[35] and recently by Lam *et al.*[36] for self-diffusion along dislocations in bulk single crystals of Te and Ag, respectively. (Presumably this was done because an exact solution, analogous to Whipple's,[27] is not currently available for isolated dislocations.) In the present case of Au films the dislocation arrangement is random[17] and the spacing is much smaller (~ 500 Å) than 10 000 Å expected in bulk crystals on the basis of a dislocation density of $\sim 10^8$ cm^{-2} and a random geometry. Therefore, the application of the homogeneous slab geometry coupled with Whipple's exact solution should be significantly better. The resulting combined parameters P_b (cm^3/sec) for dislocation-pipe diffusion follow an excellent Arrhenius temperature dependence, as may be seen in Fig. 4, having the diffusion parameters $P_b^0 = 1.9\times10^{-10}$ cm^3/sec and $Q_b = 1.16 \pm 0.02$ eV.

The solution for Smoluchowski's isolated dislocation model has the advantage that it leads directly to the cross-sectional area of the dislocation A_d, but it requires an initial assumption on the dislocation core radius r_0 in Eq. (7). It may be taken as the radius of the Au atom at 1.44 Å. It turns out that the initial assumption for r_0 does not change the subsequent value of A_d drastically since even an order-of-magnitude change in r_0 hardly doubles ϕ and consequently A_d. The combined parameters P_d (cm^4/sec) computed from Eq. (7), however, deviate from an Arrhenius plot as seen in Fig. 4, and particularly the P_d values at 352 and 352 °C are off. The source of the deviation may be the Fisher approximation in Eq. (7) in taking the flow of tracer to be purely radial outside the core and none inside.[37] The lower values of β, 120 and 335 at, respectively, 352 and 325 °C diffusion anneals, may consequently be responsible for the departure from linearity. The lower temperature data at 295.4, 275.0, and 247.5 °C for which $\beta > 1000$ remain unaffected. The preceding set of three points yields dislocation-pipe-diffusion parameters $Q_d = 1.2 \pm 0.1$ eV and $P_d^0 \sim 1.0\times10^{-17}$ cm^4/sec, which may be compared with $Q_b = 1.16 \pm 0.02$ eV and $P_b^0 \times l_d \sim 10^{-15}$ cm^4/sec (Table II) obtained previously using the homogeneous boundary condition. The two sets are in fair agreement since the precision of the preexponential terms is ordinarily within an order of magnitude.

Comparison of the activation energies for dislocation pipe diffusion and self-diffusion in Au leads to the ratio $Q_d/Q_l = 0.63$, where $Q_l = 1.81$ eV.[24] The magnitude of this ratio is significant with respect to the structure of the dislocations. Balluffi[2] has concluded that a ratio in the vicinity of 0.4 would be expected for complete or nonextended dislocations in fcc metals, whereas this ratio would be larger (0.6–0.8) for dislocations which dissociate into pairs of partials. The tendency for dissociation is the greatest for edge dislocations with a ⟨211⟩ Burger vector. A higher activation-energy ratio reflects the relaxed state of dislocation cores in extended dislocation. Relatively low stacking-fault energy in Au coupled with the ⟨211⟩-type edge dislocations present in films should favor extended dislocation configuration. The observation of $Q_d/Q_l = 0.63$ in Au is thus reasonable and compares well with the other fcc metals, notably Ni and Al, for tilt boundaries containing ⟨211⟩ edge dislocations.[3,6,8–10]

The value of the combined preexponential parameter P_d^0 in this investigation lies in the range 10^{-15}–10^{-17} cm^4/sec. A mean value of 5×10^{-16} cm^4/sec falls in the middle of the range of data summarized in Ref. 2. Since it is not possible to measure the effective cross-sectional area of the dislocation core A_d independently in tracer experiments involving sectioning, it can only be estimated from the knowledge of D_d^0, since $P_d^0 = A_dD_d^0$. If a highly correlated vacancy mechanism is assumed for self-diffusion along dislocations, D_d^0 may be related to the lattice preexponential factor D_l^0 as

$$D_d^0 \approx f_d\, D_l^0, \tag{11}$$

where f_d is the correlation factor for tracer dif-

fusion in the dislocation core. While nothing is known with certainty about D_d^0, it should be considerably smaller than the corresponding value of $D_l^0 = 0.091$ cm^2/sec in the lattice if diffusion is to be restricted in and around the dislocation cores. A temperature-independent value of $f_d = 0.54$ in ⟨001⟩ bicrystal of Ag has recently been reported and, consequently, a value of $D_d^0 = 0.05$ cm^2/sec may not be too unreasonable. The effective cross-sectional area of the dislocation cores is, therefore, estimated at $\sim 10^{-14}$ cm^2, with a corresponding effective diameter of about 10 Å. Consequently, the dislocation core may be regarded to extend to only 3 or 4 atomic diameters for the purpose of self-diffusion, which means that diffusion is highly localized to the core. On the whole, the data of this investigation seem to follow the general pattern of self-diffusion along dislocation in other fcc metals considered in Ref. 2, and a vacancy diffusion mechanism is likely.

C. Enhanced Lattice Diffusion and Dislocation Density

Since enhanced lattice diffusion and dislocation-pipe diffusion have been adequately resolved in the penetration profiles themselves, it should be possible to account for the enhancement quantitatively according to Eq. (9). From the knowledge of D_d, which is an independently measured quantity in this investigation, either f and hence the dislocation density ρ_d may be computed, or alternatively D_l may be obtained if ρ_d is known for each specimen. The former approach is adopted to remain within the scope of this paper and also since the dislocation densities are presently not available for each specimen.

Values of the dislocation-pipe diffusivity D_d were obtained from Table II for the homogeneous slab geometry assuming $\delta = 1.5 \times 10^{-8}$ cm. The calculation of the fraction of atoms f in the dislocation pipes and hence of the dislocation density $\rho_d = f/\pi r_0^2$ is then a straightforward procedure. The resulting values of f and ρ_d are listed in Table I. It may be noted that the precision of these calculations is high since both D_{app} and δD_d are measured in the same specimen under identical conditions of temperature and time and the only assumption involved is on the magnitude of δ, which is valid within a factor of about 3. The dislocation density should also be accurate within a factor of 3 and certainly within an order of magnitude. It may be noted in passing that enhancement of lattice diffusion by the hydrostatic component of biaxial tensile stresses, of the order of 1 kbar, present in the epitaxial film is estimated at 20–30% assuming an activation volume of 7.0 cm^3/mole [38] for pressure-dependent diffusion in Au. It is negligibly small in comparison to the dislocation enhancement of severalfold.

The average dislocation density of $\sim 10^{11}$ cm^{-2} in the epitaxial Au films obtained from self-diffusion measurements compares quite favorably with the observed dislocation density[17,18] in the range 10^{10}–10^{11} cm^{-2}. There is an unmistakable temperature dependence in the observed values of f and ρ_d, as may be seen in Table I where both drop systematically with decreasing temperatures of diffusion annealing. It stems from the unexpectedly large value of activation energy for D_{app} at 1.73 eV being only slightly smaller than Q_l. Ordinarily, the dislocation densities should be temperature independent since the film growth was at 450 °C—much higher than the diffusion temperatures—and the activation energy for D_{app} should be an average of the activation energies Q_l and Q_d determined by the Eq. (9). A qualitative explanation of the above observation appears to be an appreciable thermal vibrational motion of the dislocations, alluded to earlier (Sec. IV A), which could have imparted a temperature dependence to ρ_d by short circuiting a larger number of tracer atoms.

V. CONCLUSIONS

It has been demonstrated for the first time that lattice self-diffusion and rapid diffusion along dislocations can be uniquely resolved in the penetration profiles themselves by restricting the diffusion distance $(D_l t)^{1/2}$ to about 100 Å at temperatures below $0.5T_m$. Material removal by rf sputtering is found to be highly successful for profiling radioactive tracers on a submicron scale. The use of (001) single-crystal Au films yielded precise diffusion data in the lattice as well as along dislocations. The data for self-diffusion along dislocations were analyzed using the homogeneous slab geometry as well as the isolated dislocation geometry. Both yield equivalent results at low temperatures where β is large. The activation energy Q_d and the combined preexponential factor $A_d D_d^0$ are found to be 1.16 ± 0.02 eV and 5×10^{-16} cm^4/sec, respectively. From the magnitude of the diffusion parameters for dislocations, it is concluded that ⟨211⟩ dislocations present in Au single-crystal films are extended and self-diffusion takes place very near to the dislocation cores; the latter is indicative of a vacancy mechanism. Finally, from the enhanced lattice diffusion in the first stage of the penetration profile, it was possible to evaluate the film dislocation density at $\sim 10^{11}$ lines/cm^2.

ACKNOWLEDGMENTS

The author is grateful to Dr. R. Rosenberg for introducing him to the field of thin films and for many stimulating discussions. He wishes to thank K. W. Asai for help in diffusion measurements.

J. J. Cuomo for Au film preparation, and P. A. Roland for carrying out computations. Helpful discussions with Dr. B. S. Berry and Dr. D. R. Campbell are also acknowledged.

[1]P. G. Shewmon, *Diffusion in Solids* (McGraw-Hill, New York, 1963), p. 174.
[2]R. W. Balluffi, Phys. Status Solidi 42, 11 (1970).
[3]M. Wuttig and H. K. Birnbaum, Phys. Rev. 147, 495 (1966).
[4]C. Baker, M. Wuttig, and H. K. Birnbaum, Trans. Japan Inst. Metals Suppl. 9, 268 (1968).
[5]D. Turnbull and R. E. Hoffman, Acta Met. 2, 419 (1954).
[6]R. F. Canon and J. P. Stark, J. Appl. Phys. 40, 436 (1969).
[7]W. R. Upthegrove and M. J. Sinnot, Trans. ASM 50, 1031 (1958).
[8]E. C. Oren and C. L. Bauer, Acta Met. 15, 773 (1967).
[9]T. E. Volin, K. H. Lie, and R. W. Balluffi, Acta Met. 19, 263 (1971).
[10]J. T. Robinson and N. L. Peterson, Surface Sci. 31, 586 (1972).
[11]A. Seeger and H. Mehrer, Phys. Status Solidi 29, 231 (1968).
[12]T. G. Stoebe and H. T. Dawson, Phys. Rev. 166, 621 (1968).
[13]W. Rupp, U. Ermert, and R. Sizmann, Phys. Status Solidi 33, 509 (1969).
[14]J. L. Whitton and G. V. Kidson, Can. J. Phys. 46, 2589 (1968).
[15]H. M. Morrison and V. L. S. Yuen, Can. J. Phys. 49, 2704 (1971).
[16]J. W. Matthews, Phil. Mag. 4, 1017 (1959).
[17]D. W. Pashley, Phil. Mag. 4, 324 (1959).
[18]D. Gupta and R. T. C. Tsui, Appl. Phys. Letters 17 294 (1970).
[19]D. Gupta (unpublished).
[20]Marz-grade Au was obtained from Materials Research Corp., Orangeburg, N. Y.
[21]The author is grateful to J. Angilello for carrying out Laue x-ray diffraction on Au films, and to C. F. Aliotta for examining the surfaces under electron microscope.
[22]Carrier-free Au^{195} was obtained from New England Nuclear, Boston, Mass.
[23]R. T. C. Tsui, Semicond. Proc. 10, 33 (1967).
[24]S. M. Makin, A. H. Rowe, and A. D. LeClaire, Proc. Phys. Soc. (London) 70, 545 (1957).
[25]J. C. Fisher, J. Appl. Phys. 23, 74 (1951).
[26]R. T. P. Whipple, Phil. Mag. 25, 1225 (1952).
[27]R. Smoluchowski, Phys. Rev. 87, 482 (1952).
[28]P. V. Pavlov *et al.*, Fiz. Tverd. Tela 6, 382 (1964) [Sov. Phys. Solid State 6, 305 (1964)].
[29]G. Brebec, Centre D'Etudes Nucleaires de Saclay Report No. CEA-R 2831, 1965 (unpublished).
[30]L. G. Harrison, Trans. Faraday Soc. 57, 1191 (1961).
[31]E. W. Hart, Acta Met. 5, 597 (1957).
[32]A. L. Ruoff and R. W. Balluffi, J. Appl. Phys. 34, 1848 (1963).
[33]C. T. Lai and H. M. Morrison, Can. J. Phys. 48, 1548 (1970).
[34]H. M. Morrison, Phil. Mag. 12, 985 (1965).
[35]R. N. Ghostagore, Phys. Rev. 155, 603 (1967).
[36]N. Q. Lam, S. J. Rothman, and L. J. Nowicki, Bull. Am. Phys. Soc. 17, 244 (1972).
[37]N. A. Gjostein, in *Techniques of Metals Research*, edited by R. A. Rapp (Interscience, New York, 1970), p. 447.
[38]M. Beyeler and Y. Adda, J. Phys. (Paris) 29, 345 (1968).

PHYSICAL REVIEW B VOLUME 7, NUMBER 2 15 JANUARY 1973

Anharmonicity in Noble Metals; Nonlinear Elasticity in Whiskers

Hiroshi Kobayashi* and Yosio Hiki
Tokyo Institute of Technology, Oh-okayama, Meguro-ku, Tokyo, Japan
(Received 6 March 1972)

A nonlinear stress-strain relation has been observed in copper whiskers with [100], [110], and [111] orientations using a sensitive apparatus for tensile-stress measurement. The nonlinearity was considered to be due to the lattice anharmonicity of the crystal. The nonlinearity constants of the specimens, which represent the amount of the deviation from linear elasticity, have been found to depend apparently on their yield stresses. Whiskers with low yield stresses showed large values of the nonlinearity constants. It was assumed that there was some kind of defects on the specimen surfaces and that the stress concentrations near the defects produced by the external forces lowered the yield stresses and increased the apparent nonlinearity constants. A simple analysis based on this assumption was enough to explain the experimental results, and the true nonlinearity constants which should be possessed by crystals without defects have been evaluated. The values of the true nonlinearity constants thus determined experimentally for three crystal orientations were consistent with the theoretical values from higher-order elasticity theory.

I. INTRODUCTION

The lattice vibrations of crystals are naturally anharmonic and some of the thermal, mechanical, and acoustic properties of solids are influenced markedly or are determined entirely by the lattice anharmonicity.[1-4] A continuum or elastic approximation can be adopted for treating the crystal an-